ISSN 2347 - 3983
Volume 5, No.6 June 2017
International Journal of Emerging Trends in Engineering Research
Available Online at http://www.warse.org/IJETER/static/pdf/file/ijeter01562017.pdf

A linear-elastic linear-plastic approach for the forming simulation of sandwich sheets with cohesive elements

Benedikt Poggel[1], Bernd Engel[2]
[1]Kirchhoff Automotive Deutschland GmbH, Germany, benedikt.poggel@kirchhoff-automotive.com
[2]University of Siegen, Chair of forming technology, Germany, bernd.engel@uni-siegen.de

ABSTRACT

One possibility to achieve lightweight construction is the use of sandwich sheets. In this paper die behavior of the interface layer between steel and core is analyzed with single lap shear tests. The relation between adhesion promoter thickness and shear strength is carried out. Based on the experimental results a linear-elastic linear-plastic interpolation approach was suggested and transferred to a user material routine with cohesive elements in LS-Dyna. With consideration of the user material the single lap shear tests were simulated

Key words : sandwich sheet, adhesion promoter, user material, cohesive elements.

1. INTRODUCTION

Lightweight construction plays an increasingly important role in automotive industry. In addition to new steel generations or aluminum, hybrid materials like sandwich sheets are also a possibility to achieve a weight reduction in the car body [1], [2]. Due to the sandwich material with several layers of different materials over the sheet thickness (Figure 1), the production of components made of sandwich material puts high demands on process design and forming [3].

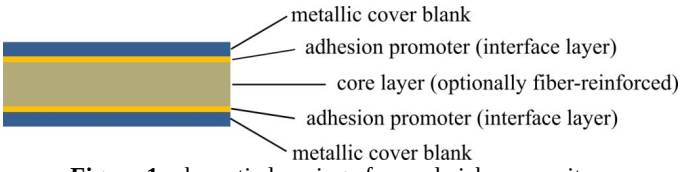

Figure 1 schematic layering of a sandwich composite

Compared to the forming of monolithic steel blanks the forming of sandwich sheets is more complex [4]. According to [5] in addition to the known failure modes like wrinkling and cracking due to the forming process of steel blanks the failure of the sandwich core has to be considered. Failure modes like delamination in the interface layer between the sandwich core and the metallic cover blanks or a failure of the core layer can occur. In previous investigations the core layer of a sandwich sheet was modeled by Mosse with shell elements [6]. The connection to the coversheet was represented with a friction based contact. Another way to model the core layer are solid elements with a tied connection to the coversheets or a multi-layered shell approach, were all layers of the sandwich sheet are reduced to one shell element with different properties in every integration point [7]. The modelling approach with solid elements is very accurate, but it has the main disadvantage of long simulation times due to the time step dependence of the element thickness. A multi-layered shell approach is much faster but also inaccurate. All approaches have in common that there is no consideration of the adhesive interlayer, which is one of the weak points of the sandwich material.

For the consideration of the failure in the interface layer single lap shear specimens are prepared with an adhesion promoter interlayer without an additional core. During the consolidation phase of the sandwich specimens different interlayer thicknesses were established. Based on the single lap shear tests the correlation between interlayer thickness and shear stress respectively shear strain is pointed out. Afterwards a simple analytic model is established to describe the correlation between shear stress and shear strain. The analytic model is transferred to a user material routine in LS-Dyna and FE simulations of the single lap shear specimens are performed.

2. EXPERIMENTAL WORK

As base material a HC340 LA is used. The chemical composition according to DIN EN 10268 is presented in Table 1 .

Table 1 chemical composition of HC340 LA in wt % [8]

max. C	max. Si	max. Mn	max. P	max. S	min. Al	max. Ti	max. Nb
0,12	0,5	1,5	0,03	0,025	0,015	0,15	0,09

For the simulation the material needs to be characterized to obtain stress strain curves. Therefore the sheet metal is milled to A50 tensile tests. The tensile tests were performed according to DIN EN ISO 6892-1 A1 [9] on a Zwick/Roell Z250 universal testing machine. The test speed was controlled by a local displacement transducer and was set to a constant strain rate of v = 0.00025 1/s in the elastic area and a strain rate of v = 0.0067 1/s in the plastic area up to failure. The results can be obtained in Figure 2.

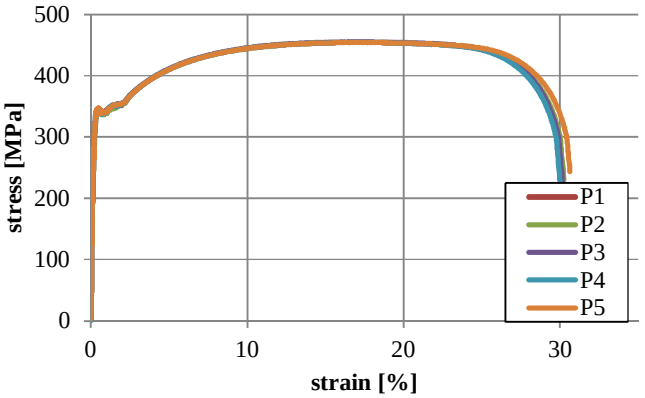

Figure 2 Stress Strain curve for CR340LA t = 2,5 mm from tensiletest and interpolation according Swift Krupkowski

For the input to the simulation the average values of the parameters Rm, Rp0,2 and Ag, respectively the effective strain φe were calculated. Afterwards the stress-strain curve according to Swift-Krupkowski [10] was generated (Eq. 1). The material-specific values determined are listed in Table **2**.

$$k_f = b * (c + \varphi_v)^d \qquad \text{Eq. 1}$$

Table 2 material-specific values determined in tensile test

Rp0,2 [MPa]	s [MPa]	Rm [MPa]	s [MPa]	Ag [%]	s [%]
341,1	1,4	454,4	0,3	16,8	0,3

To determine the properties of the adhesion-promoting layer, iron-phosphated sheets of CR340 LA were coated on one side with an adhesion promoter. The adhesion promoter is based on a copolyamide. Afterwards two sheets were consolidated to one single lap shear specimen. For the consolidation process an electrically heated plate tool (Figure 3) was used. In order to control the tool displacement and the press force the tool was mounted in a Zwick Roell Z250.

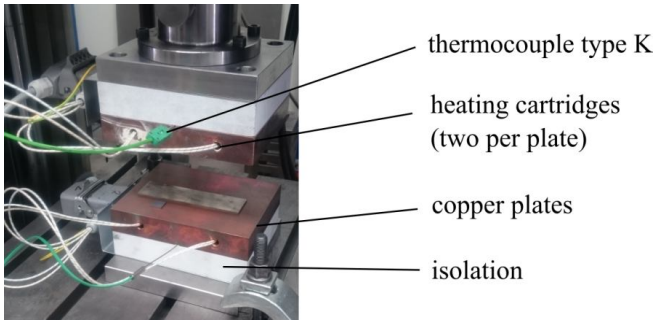

Figure 3 tool setup for consolidation of specimen

Within the scope of a parameter study, the process parameters for the consolidation process listed in Table 3 were defined in advance.

Table 3 parameter set for manufacturing the test specimens

	temperature T [°C]	compression time tc [s]	layer thickness sap [mm]
set 1	190	90	0,1; 0,12; 0,16; 0,22

The dimensions of the shear tensile specimen were specified in accordance to DIN EN 1465 [11]. The overlap length of 20 mm was previously determined by FE simulations with an assumed shear strength of 25 MPa.
In addition to the tensile load in the specimen, a bending moment is introduced in the specimen which leads to a peel stress in the adhesion-promoter layer [12]. In order to reduce peel stress a sufficient thickness of 2,5 mm of the base material was used.
Figure 4 shows four representative shear stress strain curves of the shear tensile tests. The thickness of the adhesion promoter was varied and all other process parameters during the consolidation like temperature and pressing time were kept constant. As the thickness of the adhesion-promoting layer increases, the maximum shear strength of the compound decreases. At the same time, the maximum displacement increases with increasing adhesion promoter thickness.

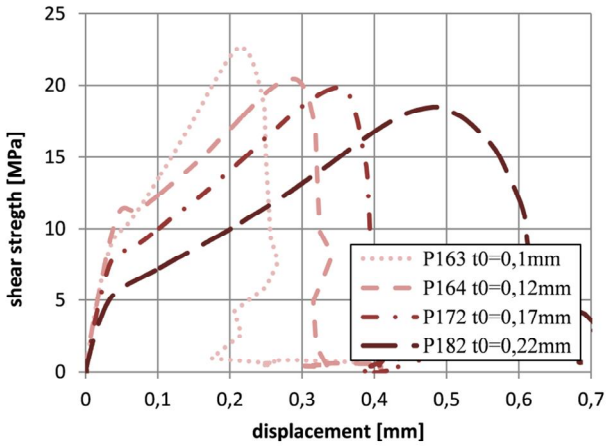

Figure 4 shear strength displacement diagram for shear specimen with a different core layer thickness

Since the shear strain γ is defined as the quotient of displacement dl and the initial adhesion promoter thickness sap the shear strain remains almost constant while the adhesion promoter thickness is varied (Figure 5). Similar results could be obtained in [13], [14] for epoxy resin based structural adhesives.

$$\gamma = \frac{dl}{s_{ap}} \qquad \text{Eq. 2}$$

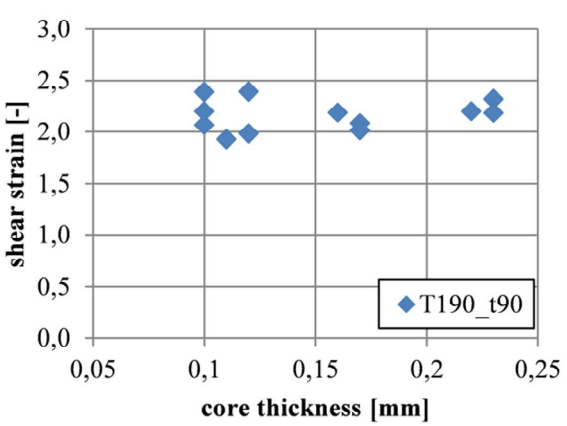

Figure 5 shear strain as a function of adhesion promoter thickness (T =190 °C; t = 90 s)

3. NUMMERICAL APPROXIMATION

The measured shear stress strain curves can be separated analog to the tensile test in two sections (Figure 6). On the one hand an elastic section up to $\tau(\gamma) < \tau_{p0,1}$, where the shear modulus G can determined. On the other hand a section with plastic deformation where the material strengthens up to failure. This section is determined by $\tau_{p0,1} < \tau(\gamma) < \tau_{max}$.

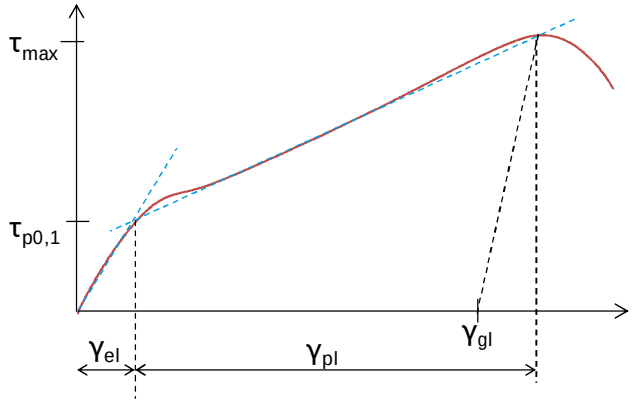

Figure 6 schematic shear stress shear strain curve with linear interpolation

For the approximation of the obtained shear stress strain curves, a linear approach consisting of two straight lines was selected (Figure 6). The shear modulus G was determined by a tangent which was placed through the point with the maximum gradient of the shear stress strain curve and the origin.

$$G = \tau\left(\frac{d^2\tau}{d\gamma^2} = 0\right) \qquad \text{Eq. 3}$$

For the approximation in the section with plastic deformation a straight line was placed through the point at $\tan(\gamma) = 0{,}5$ and the point with the maximum shear strength τ_{max}.

$$m = \frac{\tau_{max} \quad \tau_{0,5}}{\gamma_{max} \quad \gamma_{0,5}} \qquad \text{Eq. 4}$$

The intersection with the y-axis is obtained by the following eq.

$$b = \tau_{max} - m * \gamma_{max} \qquad \text{Eq. 5}$$

The equation for the plastic deformation is defined by Eq. 6

$$\tau_{pl}(\gamma) - \frac{\tau_{max} - \tau_{0,5}}{\gamma_{max} - \gamma_{0,5}} * (\gamma - \gamma_{max}) + \tau_{max} \qquad \text{Eq. 6}$$

With Eq. 3 and Eq. 6 the intersection of the shear modulus G with the interpolation line in the plastic deformation area is defined by

$$\gamma_{elpl} = \frac{\tau_{max} - \frac{\tau_{max} - \tau_{0,5}}{\gamma_{max} - \gamma_{0,5}} * \gamma_{max}}{G - \frac{\tau_{max} - \tau_{0,5}}{\gamma_{max} - \gamma_{0,5}}} \qquad \text{Eq. 7}$$

Respectively for the shear stress value

$$\tau_{elpl} = \gamma_{elpl} * G \qquad \text{Eq. 8}$$

The shear strain γ_{elpl} corresponds to the maximum elastic strain. The stress τ_{elpl} is set as the flow limit between the elastic and plastic area.
For the shear stress in the plastic area at $\tau > \tau_{elpl}$ the following equitation applies

$$\tau_{pl} = m * (\gamma_{elpl} + \gamma_{pl}) + b \qquad \text{Eq. 9}$$

4. FE MODEL

The shear tensile tests carried out were modeled in LS-Dyna. Cohesive elements are used to describe the core layer.
In contrast to standard solid elements, which have six independent displacement components, the considered cohesive element has only three. For the use of the displacement-reduced cohesive element, two assumptions are required [15].
On the one hand, the element does not allow lateral expansion, $\varepsilon_{xx}, \varepsilon_{yy} = 0$. On the other hand, no plane shear is allowed, $\varepsilon_{xy} = 0$.
Taking these two assumptions under consideration, the stress matrix of the cohesive element is reduced compared to the solid element (Eq. 10).

$$\begin{matrix}\sigma_{xx} & \sigma_{xy} & \sigma_{xz} \\ \sigma_{yx} & \sigma_{yy} & \sigma_{yz} \\ \sigma_{zx} & \sigma_{zy} & \sigma_{zz}\end{matrix} \rightarrow \begin{matrix}0 & 0 & \sigma_{xz} \\ 0 & 0 & \sigma_{yz} \\ \sigma_{zx} & \sigma_{zy} & \sigma_{zz}\end{matrix} \qquad \text{Eq. 10}$$

For modeling the adhesion promoter layer, the approximation shown in Eq. 3 to Eq. 9 was used. The equations were implemented in a user material routine for cohesive elements in LS-Dyna. For the stress in the normal direction, a simplified elastic approach with $\sigma_x = E*\varepsilon_x$ implemented. In this approach the elastic modulus E is determined by E = 2(1

+ nu)*G. For transverse contraction nu, a value of 0.4 was assumed for PA6 [16].
To validate the linear elastic-linear plastic approximation of the shear stress strain curve, the single lap shear test was modeled in LS–Dyna. For the steel sheets, the material card *Mat_24 (*MAT_PIECEWISE_LINEAR_PLASTICITY) [15] was used with isotropic material properties based on the flow curve approximation according Swift-Krupkowski. In the area of the clamping, the specimen was assumed to be a rigid body (*Mat_20). To evaluate the simulation, a cross section for force measurement was inserted above the clamping. On one side of the specimen all degrees of freedom were locked in the rigid body. On the opposite edge of the specimen a maximum displacement of 1,0 mm was applied to the rigid body. The failure of the specimen was modeled with a strain-based failure criterion (Eq. 11).

$$failure(\gamma) = \begin{cases} 0, & \gamma < \gamma_{pl} \\ 1, & \gamma \geq \gamma_{pl} \end{cases} \qquad \text{Eq. 11}$$

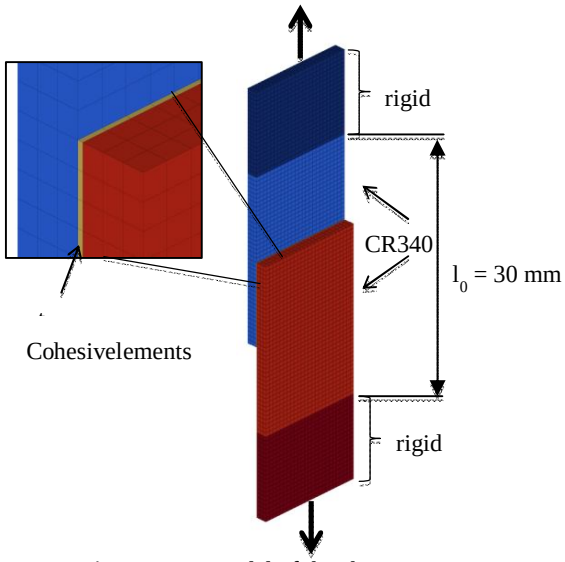

Figure 7 FE-Model of the shear strain test

5. RESULTS AND EVAUATION

The experimental tests show an increasing shear strength with a decreasing adhesion promoter thickness. Similar results were already obtained in different investigations with epoxy adhesives [13], [14].
A comparison between the experimental data and the simulation data shows a similar progress of the shear stress strain curves (Figure 8). In the area of smaller shear strains, the consistency between simulation and experiment is better. For larger shear strains, the simulated shear strength is lower than the experimental data due to the linear approximation. The point of failure is well met with the shear strain based approach.

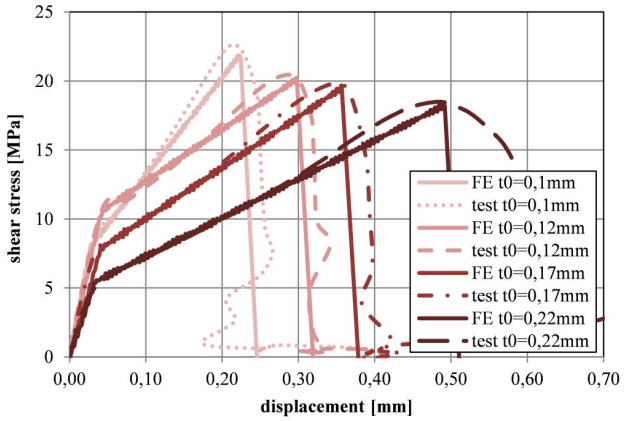

Figure 8 results of the single lap tensile test: comparison of test specimens and FE simulations

The model can be used to describe the single lap shear test and the behavior of the adhesion promoter under pure shear load. The deviation below the maximum shear stress could be caused by the previous assumption of the tension component σ_z.

6. CONCLUSION

By the use of shear lap specimens with an adhesive promoter interlayer a relation between the adhesive interlayer thickness and the resulting shear stress respectively shear strain was presented. Based on the shear lap tests a linear approximation with two straight lines was applied to the shear stress-strain cures. For a validation of the estimated model the approximation equations were transferred to a umat routine for cohesive elements in LS-Dyna. As input parameters the G Modulus, the maximum shear strength and maximum shear strain are required. Furthermore another data point (e.g. $\tau(\gamma = 0{,}5)$ in the section of plastic deformation is needed.
The FE simulation shows a good analogy compared to the performed tests. The deviation of 1,5 MPa next to the shear maximum might be caused by the simplification of the tensile stress component. By using the maximum shear strain as a failure criterion, the failure of the specimen could also be modeled in a sufficient way.
In further work the model has to be extended for the description of tensile and combined tensile shear load. Furthermore it has to be validated for the use of forming process by a validation with a typical forming geometry.

REFERENCES

1. C. Filthaut, I. Rogner, **Prozesskette im Automobilbau verkürzt**: Blechbearbeitung: Vorbeschichtetes Material erspart teure Fertigungsschritte, *Industrie Anzeiger* (11 September 2006).
2. Thyssen Krupp InCar plus, **Einsatzpotential von Litecor in der Karosserie**, *ATZ Extra* Oktober 2014 (2014).

3. T. Wollmann, C. Krbetschek, B. Poggel, O. Vogt, C. Paul, J. Jaschinski, R. Kawalla, N. Modler, **MANUFACTURING OF HIGH PERFORMANCE CARBON FIBRE-REINFORCED METAL SANDWICH MATERIALS AND THEIR FORMING BEHAVIOUR**, *ECCM17 - 17th European Conference on Composite Materials* (2016).
4. B. Poggel, R. Schwarzer, C. Paul, O. Vogt, T. Wollmann, M. Hahn, G. Meschut, S. Wiedemann, H. Wessels, H.-J. Wetterau, N. Modler, J. Jaschinski, T. Weber, R. Kawalla, C. Krbetschek, M. Oswald, M. Würtele, S. Wolf, M. Schadhauser, C. Schmal, M. Gerkens, H.-P. Vogt, A. Breidenbach, S. Reisewitz, I. Rogner, B. Lehmhaus, **Leika - effiziente Mischbauweisen für Leichtbau-Karosserien**: Abschlussbericht, Bundesministerium für Forschung und Bildung, 2017.
5. J. Buhl, **Umformeigenschaften von Sandwichblechen** (2013).
6. L. Mosse, P. Compston, W.J. Cantwell, M. Cardew-Hall, S. Kalyanasundaram, **The development of a finite element model for simulating the stamp forming of fibre–metal laminates**, *Composite Structures* 75 (2006) 298–304.
7. D. Pieronek, T. Böger, R. Röttger, **Modeling approach for steel sandwich materials in automotive crash simulations**, *11th LS-DYNA Forum* (2012).
8. DIN Deutsches Institut für Normung e.V., **Kaltgewalzte Flacherzeugnisse aus Stählen mit hoher Streckgrenze zum Kaltumformen - Technische Lieferbedingungen**, DIN EN 10268, Beuth Verlag GmbH, Berlin, 2013 (2013-12).
9. DIN Deutsches Institut für Normung e. V., **Metallic materials – Tensile testing – Part 1: Method of test at room temperature (ISO 6892-1:2016)**, first ed., 6892, Beuth Verlag GmbH, Berlin, 2017 (Februar 2017) (accessed 20 April 2017).
10. H.W. Swift, **Plastic instability under plane stress**, *Journal of the Mechanics and Physics of Solids* 1 (1952) 1–18.
11. DIN Deutsches Institut für Normung e.V., **DIN EN 1465**: Klebstoffe - Bestimmung der Zugscherfestigkeit von Überlappungsklebungen (2009).
12. G. Habenicht, **Kleben - erfolgreich und fehlerfrei**: Handwerk, Praktiker, Ausbildung, Industrie, sixth., überarb. und erg. Aufl., Vieweg + Teubner, Wiesbaden, 2012.
13. José M. Arenas, Julián J. Narbón, Cristina Alía, **Optimum adhesive thickness in structural adhesives joints using statistical techniques based on Weibull distribution**, *International Journal of Adhesion and Adhesives* (2010).
14. da Silva, Lucas F. M., Rodrigues, T. N. S. S., M.A.V. Figueiredo, de Moura, M. F. S. F., J.A.G. Chousal, **Effect of Adhesive Type and Thickness on the Lap Shear Strength**, *The Journal of Adhesion* 82 (2006) 1091–1115.
15. LIVERMORE SOFTWARE TECHNOLOGY CORPORATION, **LS-DYNA® KEYWORD USER'S MANUAL**: VOLUME II Material Models (05/26/16).
16. G. Abts, **Kunststoff-Wissen für Einsteiger**, second., aktualisierte Aufl., Hanser, München, 2014.